Remote Sensing of Environment 171 (2015) 45–57

Contents lists available at ScienceDirect

Remote Sensing of Environment

journal homepage: www.elsevier.com/locate/rse

The impact of spatial resolution on the classification of plant species and functional types within imaging spectrometer data

Keely L. Roth [a,*], Dar A. Roberts [b], Philip E. Dennison [c], Seth H. Peterson [b], Michael Alonzo [b]

[a] Department of Land, Air and Water Resources, University of California, Davis, One Shields Ave, Davis, CA 95616, United States
[b] Department of Geography, University of California, Santa Barbara, 1832 Ellison Hall, Santa Barbara, CA 93106, United States
[c] Department of Geography and Center for Natural and Technological Hazards, University of Utah, 260 S Central Campus Dr., Room 270, Salt Lake City, UT 84112, United States

ARTICLE INFO

Article history:
Received 24 April 2015
Received in revised form 30 September 2015
Accepted 8 October 2015
Available online xxxx

Keywords:
Hyperspectral
Species classification
Plant functional types
Scaling
Canonical discriminant analysis

ABSTRACT

Several upcoming hyperspectral satellite sensor missions (e.g., the Hyperspectral Infrared Imager and the Environmental Mapping and Analysis Program) will greatly expand the opportunities for researchers to use imaging spectroscopy data for discriminating and mapping plant species and plant functional types (PFTs; defined in this study as combinations of leaf-type, leaf/plant duration and life form). Accurate knowledge of the spatial distribution of dominant plant species and PFTs is highly valuable to many scientific and management goals, including improved parameterization of ecosystem process and climate models, better invasive species distribution monitoring and forecasting, quantification of human and natural disturbance and recovery processes, and evaluations of terrestrial vegetation response to climate change. Most often, species-level discrimination has been achieved using fine spatial resolution (≤20 m) airborne imagery, but currently proposed spaceborne imaging spectrometers will have coarser spatial resolution (~30 to 60 m). In order to address the impact of coarser spatial resolutions on our ability to spectrally separate species and PFTs, we classified dominant species and PFTs in five contrasting ecosystems over a range of spatial resolutions. Study sites included a temperate broadleaf deciduous forest, a brackish tidal marsh, a mixed conifer/broadleaf montane forest, a temperate rainforest and a Mediterranean climate region encompassing grasslands, oak savanna, oak woodland and shrublands. Data were acquired by the Airborne Visible/Infrared Imaging Spectrometer (AVIRIS) over each site, and spatially aggregated to 20, 40 and 60 m resolutions. Canonical Discriminant Analysis (CDA) was used to classify species and PFTs at each site and across scales with overall accuracies ranging from 61 to 96% for species and 83–100% for PFTs. The results of this study show accuracy increases at coarser resolutions (≥20 m) across ecosystems, supporting the use of imaging spectroscopy data at spatial resolutions up to 60 m for the purpose of discriminating among plant species and PFTs. In four of the five study sites, the best accuracies were achieved at 40 m resolution. However, at coarser resolutions, some fine-scale species variation is lost and classes that occur only in small patches cannot be mapped. We also demonstrate that spectral libraries developed from fine spatial resolution imagery can be successfully applied as training data to accurately classify coarser resolution data over multiple ecosystems.

1. Introduction

Ecosystem- and regional-scale maps of vegetation composition, function and health derived from remote sensing data have played a key role in measuring and monitoring changes in the natural environment across space and time (Kerr & Ostrovsky, 2003; Turner et al., 2003). In particular, these maps are used to characterize the spatial distribution of vegetation types and to monitor land cover change due to climate, natural disasters and human activity. They are also important inputs to ecosystem process and climate models (DeFries, 2008; Turner, Ollinger, & Kimball, 2004). Making these maps on a global scale is quite challenging. Most global data products are derived using coarse spatial resolution (≥500 m), multispectral data. Sensors such as the Advanced Very High Resolution Radiometer (AVHRR) and Moderate Resolution Imaging Spectrometer (MODIS) have been used to create several global land cover maps that include vegetation types based primarily on biomes (e.g., evergreen forest, woodlands, open shrublands, etc.) (DeFries, Hansen, Townshend, & Sohlberg, 1998; Friedl et al., 2002; Hansen, DeFries, Townshend, & Sohlberg, 2000; Loveland et al., 2000; Muchoney, Strahler, Hodges, & LoCastro, 1999). While biome-level maps are useful, many applications require more detailed information regarding plant functional type (PFT) composition (Bonan, Levis, Kergoat, & Oleson, 2002), because these classes are more concretely linked to biospheric processes of interest, such as carbon, water and energy fluxes (DeFries et al., 1995). Within remote sensing science, these PFTs are often defined by traits such as leaf type (e.g., broadleaf/needleleaf), leaf longevity (evergreen/deciduous) and life form

* Corresponding author.
E-mail address: klroth@ucdavis.edu (K.L. Roth).

http://dx.doi.org/10.1016/j.rse.2015.10.004

(e.g., tree/shrub/herb). Efforts to derive these products have been successful for the most part (Sun, Liang, Xu, Fang, & Dickinson, 2008; Sun & Liang, 2008), though most PFT data sets have been created using preexisting coarse-grained land cover maps (i.e., biomes). Comparison of existing global and continental classification maps is difficult because most have been made using data acquired by different sensors, or over different time periods, and often do not share the same set of classes. Assessing the accuracy of these coarse-scale maps is also challenging, given the sparseness of validation data. Finer resolution maps of vegetation composition covering smaller regions can provide improved reference data for global products. Such maps have been created using multispectral, finer spatial resolution sensors such as Landsat and SPOT (Goodenough et al., 2003; Göttlicher et al., 2009; Harvey & Hill, 2001; Price, Guo, & Stiles, 2002; Ustin et al., 1986). However, even with the global availability of finer spatial resolution data, such as Landsat (30 m), discrimination of certain PFTs and many species using broadband sensors can be difficult (Clark, Roberts, & Clark, 2005).

The most promising sensors for improving PFT maps, and even discriminating dominant plant species within PFTs, are imaging spectrometers (DeFries, 2008; Schmidtlein, Feilhauer, & Bruelheide, 2012; Ustin & Gamon, 2010; Ustin, Roberts, Gamon, Asner, & Green, 2004). Imaging spectrometers measure reflected radiance in many narrow bands, and thus are sensitive to subtle differences in plant biochemistry, physiology and structure (Kokaly, Asner, Ollinger, Martin, & Wessman, 2009; Schaepman et al., 2009; Ustin et al., 2004). These sensors have been successfully used to discriminate dominant plant species and PFTs over many types of ecosystems (Asner, 2013; Ustin & Gamon, 2010). In temperate forests, studies by Martin, Newman, Aber, and Congalton (1998), Van Aardt and Wynne (2007), and others (e.g., Plourde, Ollinger, Smith, & Martin, 2007) were able to discriminate among a wide variety of broadleaf deciduous and evergreen needleleaf tree species. In the western U.S., Goodenough et al. (2003) mapped similar functional types in a temperate forest. Kokaly, Despain, Clark, and Livo (2003) classified both species and PFTs in a mixed montane conifer forest and the surrounding shrublands, and Schaaf, Dennison, Fryer, Roth, and Roberts (2011) mapped PFTs in a similar montane ecosystem. Tropical forests, some of the most diverse ecosystems on the planet, have also been accurately classified to the species-level in many studies (Clark et al., 2005; Cochrane, 2000; Féret & Asner, 2012; Kalacska, Bohlman, Sanchez-Azofeifa, Castro-Esau, & Caelli, 2007; Somers & Asner, 2013). The successful application of imaging spectroscopy data has not been limited to forests. In Mediterranean climate shrublands, Dennison and Roberts (2003), Underwood, Ustin, and Ramirez (2007) and Roth, Dennison, and Roberts (2012) mapped PFTs and species to accuracies 75% and greater. Li, Ustin, and Lay (2005) and Pengra, Johnston, and Loveland (2007) mapped species in wetland ecosystems, and in urban areas, Zhang and Qiu (2012) and Alonzo, Roth, and Roberts (2013) were able to map single trees to the species-level. Despite these successes, these studies have been done using airborne sensors which collect data at relatively fine spatial resolutions (e.g., 4–20 m) and over limited spatial extents. This limits their applicability for monitoring vegetation on regional to global scales.

Currently, several space-borne imagining spectrometers are under development, which would provide, for the first time, global coverage. In response to data priorities from the National Research Council's Earth Science Decadal Survey (NRC, 2007), NASA's proposed Hyperspectral Infrared Imager (HyspIRI) mission includes a full visible-shortwave infrared (VSWIR) instrument which will collect data at 60 m with a 19 day repeat acquisition time (HyspIRI Team, 2009; Roberts, Quattrochi, Hulley, Hook, & Green, 2012). The German hyperspectral satellite mission Environmental Mapping and Analysis Program (EnMAP) will collect data swaths of 30 km at a ground resolution of 30 m (Kaufmann et al., 2006). Additional missions include Italy's PRecursore IperSpettrale (PRISMA), and both China and Japan are also currently developing spaceborne imaging spectrometers. These missions will greatly increase the availability of imaging spectroscopy data, leading to more comprehensive mapping of PFTs and species. While the spectral and radiometric resolutions of the many of these proposed sensors are based on existing aerial sensors, the proposed spatial resolutions will be coarser. Therefore, it is important to evaluate the impacts of spatial resolution on the discrimination of dominant species and PFTs across a wide range of ecosystems.

Determining the optimal scale for mapping vegetation properties has been an ongoing area of research in remote sensing science (Atkinson & Curran, 1995; Curran & Atkinson, 1999; Woodcock & Strahler, 1987). The scale at which observations are made (i.e., the pixel size) may or may not align well with the scale of biogeophysical processes, and target size (e.g., individual trees, patches of a given species, etc.) will vary across ecosystems and with ecological questions and concerns (Feld et al., 2009; Fisher, 1997; Turner, Neill, Gardner, & Milne, 1989). The implications of this mismatch have been widely considered, and a more in-depth discussion of these can be found in Marceau, Gratton, Fournier, and Fortin (1994), Woodcock and Strahler (1987), and Wu and Li (2009). Most importantly, image spatial resolution will have a significant impact on the ability to accurately characterize surface attributes of interest, such as land cover.

Most scaling studies have been done using data from broadband sensors (Atkinson & Curran, 1997; Chen, Stow, & Gong, 2004; Cohen, Spies, & Bradshaw, 1990; Nelson, McRoberts, Holden, & Bauer, 2009), and few imaging spectroscopy studies have examined the role of spatial scale in discriminating plant species and functional types. Here two types of scale can be considered: physical scale (e.g., leaf vs. branch vs. canopy) and image spatial resolution (i.e., pixel size). Studies by Roberts et al. (2004) in a Pacific Northwest temperate rainforest (the same forest considered in this study) and Clark et al. (2005) in tropical rainforest examined changes in species discrimination across physical scales. These studies are critical because they demonstrate how spectral separability is altered by combinations of leaf structure and biochemistry, crown architecture and canopy structure. They thus provide us a better understanding of the controls on species discrimination. Other studies have examined the impact image resolution has on classification accuracy. Treitz and Howarth (2000) used CASI data to evaluate the spatial scale of variance among forest species associations in a mixed deciduous and coniferous forest. Underwood et al. (2007) compared 4 m and spatially degraded (30 m) AVIRIS data for mapping different vegetation communities with varying levels of invasion by three target species in a mixed chaparral and sage scrub ecosystem. The image was degraded using nearest neighbor resampling, and they report a decrease in overall accuracy from 75% to 58% as resolution became coarser. Schaaf et al. (2011) also spatially degraded 20 m AVIRIS data to 40 m and 60 m for their study on PFT discrimination in a montane ecosystem, but in this case, using spatial averaging to simulate coarser resolution data. Accuracy decreased as spatial resolution was coarsened, but the use of spectral libraries derived at the finer spatial resolution (20 m) improved accuracy over spectral libraries derived at coarser spatial resolutions.

In our study, we sought to expand upon this previous research by assessing the impact of coarsening spatial resolution on the accuracy of PFT and dominant plant species classification with imaging spectroscopy data across a range of North American ecosystems. In particular, we sought to answer the following questions:

1) What effect does spatial resolution have on our ability to spectrally discriminate dominant plant species and PFT composition across a range of ecosystems using imaging spectroscopy, and how do these impacts vary by ecosystem type?
2) Can reference spectral libraries developed from finer resolution (~3–18 m) imagery be used to adequately map dominant plant species and PFTs at coarser scales?

To address these questions, we analyzed imagery acquired by the Airborne Visible/Infrared Imaging Spectrometer (AVIRIS) over five ecosystems aggregated to a range of spatial resolutions up to 60 m. At each resolution and within each ecosystem, we classified dominant plant species and PFTs using canonical discriminant analysis (CDA). We hypothesized that accuracy metrics, including kappa coefficient, overall and class-specific accuracies would vary across spatial resolutions within each site and across sites at the same resolution. We further hypothesized that as fine resolution data were aggregated from 20 m to 40 m and 60 m, within-class spectral variability would decrease, potentially leading to higher classification accuracies. However, these increases would be countered by potential decreases as boundary pixels at the edges of reference patches are aggregated into a class's signal, leading to higher frequencies of misclassification. An improved understanding of these tradeoffs is necessary to define the requirements for a global mission, but also needed to link those requirements to the patch structure of ecosystems.

2. Methods

2.1. Ecosystems and Study Sites

We analyzed data over five study regions (Fig. 1, Table 1). Each site is representative of a unique ecosystem type, with varying PFT and dominant species diversity and composition. PFT and species diversities are defined as the number of distinct plant classes at each level. Three forested sites were included, the Smithsonian Environmental Research Center (SERC), Wind River Experimental Forest (WR) and Sierra National Forest (SNEV). We also analyzed a tidal marsh site on the Louisiana Gulf coast (GULF) and a site covering a broad region of the California central coast including Santa Barbara, the Santa Ynez Mountains and the Santa Ynez valley which contains evergreen and drought-deciduous shrublands, oak woodland and savanna as well as open grasslands (SBFR). The SERC site is located in Maryland and is a closed forest dominated by deciduous broadleaf tree species, including species of *Acer*, *Carya*, *Fagus* and *Quercus*, but primarily *Liquidambar styraciflua* and *Liriodendron tulipifera*. The WR site is a temperate rainforest located in southern Washington, dominated mainly by Douglas fir (*Pseudotsuga menziesii*) and western hemlock (*Tsuga heterophylla*), but with significant areas dominated by broadleaf deciduous trees (e.g., *Acer*, *Populus*) and open clear-cuts containing herbaceous understory species. At the SNEV site, a mix of evergreen needleleaf tree species including fir (*Abies* spp.), pine (*Pinus* spp.) and incense cedar (*Calocedrus decurrens*) are dominant, as well as evergreen broadleaf trees and shrubs (*Quercus chrysolepsis*, *Arctostaphylos* spp. and *Ceanothus* spp.) and deciduous broadleaf oak (*Quercus kelloggii*). Both species and PFT diversity are higher at WR and SNEV sites than at SERC. At the GULF site, perennial herbaceous plants, such as rush (*Juncus roemerianus*) and cordgrass (*Spartina alterniflora* and *Spartina patens*), are dominant. The SBFR site is the most diverse, having dominant species from eight different PFTs, including annual herbaceous species, deciduous and evergreen broadleaf trees and drought-deciduous shrubs. See Tables 2–4 for a complete PFT and species list for each site.

Fig. 1. Five study site locations: Wind River (WR), Sierra Nevada (SNEV), Santa Barbara (SBFR), Gulf (GULF) and Smithsonian Environmental Research Center (SERC).

2.2. Data acquisition and pre-processing

Over each study region, one or more flight lines were collected using AVIRIS (Green et al., 1998) (Table 1). The acquisition date for each site was timed to try to capture peak productivity in each ecosystem, and image spatial resolution varied from ~3–18 m depending on the platform on which the sensor was flown (i.e., Twin-Otter or ER-2). AVIRIS data have 224 bands covering 350–2500 nm (10 nm full-width, half-maximum). All images were pre-processed to orthorectified radiance by NASA's Jet Propulsion Lab (JPL). They were then corrected to reflectance using either MODTRAN-derived look-up tables for path and reflected radiance (described in Roberts, Green, & Adams, 1997), ACORN (ImSpec LLC) or ATCOR-4 (Richter & Schläpfer, 2002). We removed wavelength regions with a low signal to noise ratio and/or high levels of atmospheric contamination. When necessary, further georectification was performed using high resolution aerial photos collected by the National Agriculture Imagery Program (NAIP). Reference data for both PFTs and dominant species were collected either in the field or from pre-existing stem maps and high resolution images. Patches for each class were identified and required to be composed of ≥70% of the target class. These patches, also referred to as "reference polygons", were overlain on the images and used to extract class-specific spectral libraries for each site. For a more detailed description of reference data collection, see Roth et al. (2015).

JPL's orthorectification algorithm uses nearest neighbor resampling to assign pixel centers with irregular, ray-traced (x, y, z) coordinates to a regular grid. This process can result in the duplication of spectra across multiple (adjacent) orthorectified image pixels, which can impact aggregation to coarser spatial resolution. Therefore, images were spatially aggregated to ~20, 40 and 60 m resolutions by averaging only spectrally unique (i.e., no duplicate) native resolution pixels within a window approximating the target resolution size. Because native resolution varied across sites, the interim resolutions also varied (Table 1). At each spatial resolution, the spectrum from each pixel within each reference polygon was extracted into spectral libraries for analysis (Table 5). A pixel was considered to be inside a reference polygon if its center point was contained within the polygon boundaries (Fig. 2). Polygons containing zero pixel centers at a given resolution were dropped from the analysis at that resolution.

2.3. PFT and species classification

For each study site, the native resolution, full spectral libraries were split into training and validation libraries using a stratified random sampling procedure (Roth et al., 2012) at the species-level. Each species was assigned to a PFT (Tables 2-4). Here PFTs are defined as commonly-used combinations of leaf-type (i.e., broadleaf/needleleaf), leaf/plant duration (e.g., annual, evergreen), and life form (e.g., tree, shrub) (i.e., Bonan et al., 2002). The training libraries for each site included 2–34% of the total spectra (Table 5, in parentheses). Less than 10% of reference spectra were used to train the classifier for four of the five sites. The dimensionality of each native resolution training library was reduced using canonical discriminant analysis (CDA), a technique which was found previously to achieve the best species-level separation across these sites (Roth et al., 2015). CDA is similar to principal components analysis (PCA) in that it seeks to reduce the data by finding orthogonal components (i.e., functions in CDA). However, while PCA derives these components to maximize the total variance explained by each component, CDA aims to derive functions which best maximize separation among groups (e.g., plant species) (Klecka, 1980). The number of functions derived is equal to the number of groups minus one. While the number of functions may be further sub-selected using a several approaches, here we included all derived functions at each site. A separate set of canonical coefficients were derived for species and PFTs. This was done in order to allow the CDA algorithm to optimize the functions based on the set of classes to be discriminated. Each set of coefficients was applied to the

Table 1
Study site descriptions and imagery acquisition dates and spatial resolutions.

Site	Ecosystem type	Acquisition date	Native spatial resolution	20 m resolution	40 m resolution	60 m resolution	Spatial extent (sq. km)
Smithsonian Environmental Research Center (SERC)	Temperate, broadleaf, deciduous forest	2006-May-29	3.5 m	17.5 m	38.5 m	59.5 m	24
Louisiana Gulf (GULF)	Tidal marsh	2010-May-06	18 m	18 m	36 m	54 m	8996
Wind River Experimental Forest (WR)	Temperate coniferous, broadleaf rainforest	2003-Jul.-11	4 m	20 m	40 m	60 m	209
Sierra National Forest (SNEV)	Mixed coniferous, broadleaf montane forest	2003-Jul.-18	3.3 m	19.8 m	39.6 m	59.4 m	235
Santa Barbara (SBFR)	Mediterranean climate shrubland, woodland, grassland	2009-Jun.-17	12 m	24 m	36 m	60 m	1516

native resolution validation libraries as well as to the full 20, 40 and 60 m resolution libraries to calculate the canonical variables.

Linear discriminant analysis (LDA) was used to classify both species and PFTs for the native resolution validation libraries and the full 20, 40 and 60 m resolution libraries using the native resolution training library as training data in all cases (similar to Schaaf et al., 2011 and Roberts et al., 2012). LDA derives linear combinations of the canonical variables which best correlate with class membership (Fisher, 1936) and has been widely used to classify spectral data to the species-level (Clark et al., 2005; Féret & Asner, 2012; Pu, 2009). Class separability was evaluated using the kappa coefficient (Congalton, 1991), overall accuracy and class-level producer's and user's accuracies. The kappa coefficients between pairs of spatial resolutions were significance tested using z-scores (Schaaf et al., 2011). It is important to note that although some classes disappeared from the spectral libraries (at resolutions in which no reference polygons contained pixels), training signatures from all classes were used at each resolution.

3. Results

3.1. Library size and representation across scales

As Table 5 shows, the number of spectra and polygons for each site decreased substantially as spatial resolution was coarsened. Because the native resolution of the GULF site data was 18 m, these values are placed under 20 m resolution in Table 5 and in subsequent tables. The number of spectra in each library at the finest resolution ranged from 3442 (GULF) to 44,325 (SNEV), and from 38 (SERC) to 1940 (SBFR) at 60 m. At SBFR, GULF and SNEV, >85% of reference polygons persisted at all spatial resolutions. However, at SERC and WR, the number of reference polygons decreased across resolutions, retaining only 17% and 44% of reference polygons at 60 m resolution, respectively.

Across sites, as resolution was coarsened, class diversity (i.e., PFT or species diversity plus additional non-vegetation classes) was lost based on the number and size of reference polygons associated with each class. At SBFR and SNEV, all species and PFT classes were present at all spatial resolutions. At SERC, WR and GULF, the number of classes decreased, with each site losing up to five species and up to two PFT classes. At SERC, species classes not present at coarser resolutions included both uncommon dominants and frequent dominants that occur only in small patches. For the GULF site, senesced vegetation and the various classes of water were not present in libraries beyond 20 m. Though the water classes are present at coarser resolutions, the reference polygon set used in this study contained only small water class polygons, which were removed from the analysis when they no longer contained at least one pixel center. Given the aim of this study was to evaluate species and PFT discrimination accuracy, this loss was deemed acceptable. All other classes at the GULF site persisted across resolutions. WR results were similar to SERC, as infrequently dominant species or

Table 2
Summary of plant functional types and dominant species and cover types represented within the SERC & GULF sites.

Plant functional type	Species or cover	Common name
SERC		
Annual herbaceous	Crop	n/a
Senesced annual herbaceous	Crop residue/senesced grass	n/a
Deciduous broadleaf tree	*Acer* spp.	Maple
	Carya spp.	Beech
	Fagus spp.	Hickory
	Liquidambar styraciflua	Sweetgum
	Liriodendron tulipifera	Tulip poplar
	Platanus occidentalis	Sycamore
	Quercus spp.	Oak
Evergreen needleleaf tree	*Pinus* spp.	Pine
n/a	Soil	n/a
GULF		
Evergreen broadleaf shrub	*Avicennia germinans*	Mangrove
Perennial herbaceous	*Distichlis spicata*	Saltgrass
	Juncus roemerianus	Needlegrass rush
	Phragmites australis	Common reed
	Spartina alterniflora	Smooth cordgrass
	Spartina patens	Saltmeadow cordgrass
Senesced vegetation	Senesced vegetation	n/a
n/a	Clear water	n/a
	Dark water	n/a
	Sun glint	n/a
	Muddy water	n/a

Table 3
Summary of plant functional types and dominant species and cover types represented within the WR & SNEV sites.

Plant functional type	Species or cover	Common name
WR		
Senesced annual herbaceous	Senesced grass	n/a
Deciduous broadleaf shrub	*Acer circinatum*	Vine maple
Deciduous broadleaf tree	*Acer macrophyllum*	Bigleaf maple
	Alnus rubra	Red alder
	Populus trichocarpa	Black cottonwood
Evergreen needleleaf tree	*Abies grandis*	Grand fir
	Pseudotsuga menziesii	Douglas fir
	Thuja plicata	Western redcedar
	Tsuga heterophylla	Western hemlock
Perennial herbaceous	*Pteridium aquilinum*	Bracken fern
n/a	Rock or soil	n/a
SNEV		
Deciduous broadleaf tree	*Quercus kelloggii*	Black oak
	Salix spp.	Willow
Evergreen broadleaf shrub	*Arctostaphyos* spp.	Manzanita
	Ceanothus cordulatus	Mountain whitethorn
Evergreen broadleaf tree	*Quercus chrysolepsis*	Canyon live oak
Evergreen needleleaf tree	*Abies concolor*	White fir
	Abies magnifica	Red fir
	Calocedrus decurrens	Incense cedar
	Pinus jeffreyi	Jeffrey pine
	Pinus lambertiana	Sugar pine
	Pinus ponderosa	Ponderosa pine
	Sequoiadendron giganteum	Giant sequoia
Annual herbaceous	Mixed meadow	n/a
n/a	Rock	n/a

Table 4
Summary of plant functional types and dominant species and cover types represented within the SBFR site.

Plant functional type	Species or cover	Common name
SBFR		
Annual herbaceous	Irrigated grasses	n/a
	Brassica nigra	Black mustard
	Mediterranean annual grasses and forbs	n/a
Deciduous broadleaf tree	*Platanus racemosa*	Sycamore
	Quercus douglasii	Blue oak
Drought-deciduous shrub	*Artemisia californica-Salvia leucophylla*	California sagebrush-purple sage
Evergreen broadleaf shrub	*Arctostaphylos* spp.	Manzanita
	Baccharis pilularis	coyote bush
	Ceanothus cuneatus	Buckbrush
	Ceanothus megacarpus	Bigpod ceanothus
	Ceanothus spinosus	Greenbark ceanothus
Evergreen broadleaf tree	*Citrus* spp.	Lemon or orange
	Eucalyptus spp.	n/a
	Persea americana	Avocado
	Quercus agrifolia	California live oak
	Umbellularia californica	California bay laurel
Evergreen needleleaf shrub	*Adenostoma fasciculatum*	Chamise
	Eriogonum fasciculatum	California buckwheat
Evergreen needleleaf tree	*Pinus sabiniana*	Gray pine
Perennial herbaceous	Marsh/wetland	n/a
n/a	Rock	n/a
	Bare soil	n/a
	Urban	n/a

those occurring only in small patches disappeared from the classification at coarser resolutions.

3.2. PFT classifications

Overall classification accuracies for PFTs were quite high, ranging from 83 to 99.7% across study sites and spatial resolutions (Table 6). The lowest accuracies were achieved with native resolution data for all sites but the GULF, and with the exception of SNEV, PFT accuracies changed very little in response to changing spatial resolution. For SERC and SBFR, the highest PFT level accuracies were at 40 m, and for WR and GULF, at 20 m. SNEV accuracy was highest at 60 m. Significant ($p = 0.001$) improvements in kappa were found between native and 20 m resolution for SERC, SNEV and SBFR. From 20 to 40 m resolution, a significant increase in kappa was found for the SERC site, and a significant decrease in kappa for the GULF site. No significant changes in kappa occurred from 40 to 60 m resolution.

Discrimination among PFTs at SERC (Table 7) was very high at all spatial resolutions (producer's accuracies from 82 to 100% and user's accuracies form 92–100%), with the exception of the evergreen needleleaf tree class at native resolution (3.5 m). The accuracy for this PFT increased from native resolution to 20 m, and then the class disappeared from the analysis at subsequent resolutions. Accuracies for all PFTs

Table 5
Number of reference polygons and number of spectra at each resolution per site. Values in parentheses indicate training library sample size. Note: Because GULF native resolution is 18 m, it is placed under "20 m" heading.

		Native (3.3–12 m)	20 m	40 m	60 m
SERC	Spectra	9800 (906)	518	104	38
	Polygons	111	94	38	19
Gulf	Spectra	–	3442 (1165)	1656	1020
	Polygons	–	141	131	131
WR	Spectra	23,886 (1047)	1230	327	153
	Polygons	134	102	77	59
SNEV	Spectra	44,325 (790)	2524	694	315
	Polygons	79	78	77	69
SBFR	Spectra	39,946 (3749)	11,135	5118	1940
	Polygons	385	385	382	371

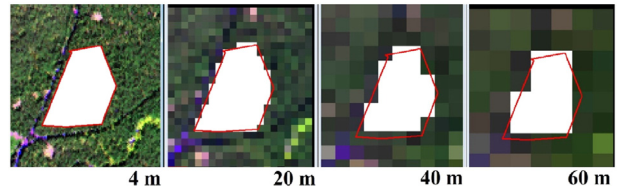

Fig. 2. The figure illustrates the inclusion or exclusion of reference patch edge pixels in accuracy assessment. Pixels whose centers fall within the patch boundaries are included.

increased with coarsening spatial resolution. A decrease in producer's accuracy was observed for SOIL at 60 m resolution, though user's accuracy remained stable. This was likely due to confusion with the green crop (annual herbaceous) class, where a comparable decrease in user's accuracy was noted at 60 m.

Discrimination was similarly high among PFT classes at the GULF site (Table 8), with producer's and user's accuracies of >97% for all classes at all resolutions, except for the evergreen broadleaf shrub class. Producer's accuracies for this class decreased considerably (96% to 79%) as resolution coarsened. A similar, but weaker, pattern was observed for its user's accuracies. User's accuracies for the perennial herbaceous class also decreased slightly (~3%) from 20 to 60 m resolution.

At WR, the average producer's accuracy across all PFTs at all resolutions was 97% and the average user's accuracy was 96% (Table 9). All PFT classes had producer's accuracies >90% and most did not change greatly across spatial resolutions. Producer's accuracy for the deciduous broadleaf tree class decreased slightly at 40 and 60 m resolutions, and the perennial herbaceous class had the lowest accuracy at 20 m resolution (75%). User's accuracies increased substantially for the deciduous broadleaf shrub, perennial herb and rock/soil classes between native and 20 m resolution, then stabilized or decreased very slightly at coarser resolutions.

Within the SNEV site, individual PFT class accuracies varied more so than at the previously described sites (Table 10). Evergreen needleleaf tree, annual herbaceous and rock classes had producer's and user's accuracies ≥87% at all spatial resolutions. Lower accuracies were achieved for the deciduous broadleaf tree, evergreen broadleaf shrub and evergreen broadleaf tree classes (producer's accuracies from 57 to 86% and user's accuracies from 28 to 73%). Both producer's and user's accuracies increased from native to 20 m resolution for all PFTs. Beyond this initial increase, however, values varied only slightly for most PFTs. Of the six classes at this site, two had their highest producer's accuracy at 20 m and 40 m. Four classes had their highest user's accuracy at 60 m resolution.

At SBFR, producer's accuracies across scales were all ≥70% with the exception of the evergreen needleleaf tree class, which had accuracies of about 50%, increasing to around 65% at 60 m resolution (Table 11). The most accurate classes were annual herbaceous, drought-deciduous shrub, perennial herbaceous and urban cover (all producer's accuracies >90%). Discrimination of evergreen functional types (broadleaf shrub, broadleaf tree and needleleaf shrub) was somewhat lower (70–82%). Producer's accuracies for several classes increased very slightly at courser resolutions, but for the majority of PFTs, accuracies changed very little.

Table 6
Kappa coefficients and % overall accuracies (OA) for PFT classifications. Bold values indicate the highest kappa for each row. Asterisks denote significant differences from previous resolution (*$p = 0.05$, **$p = 0.01$, ***$p = 0.001$).

	Native		20 m		40 m		60 m	
PFTs	Kappa	OA	Kappa	OA	Kappa	OA	Kappa	OA
SERC	0.92	94%	0.97***	97%	**1.00*** **	99%	0.96	97%
GULF	–	–	**0.99**	100%	0.83***	97%	0.78	97%
WR	0.98	99%	**0.99**	100%	0.97	99%	0.97	99%
SNEV	0.73	83%	0.83***	90%	0.83	90%	**0.84**	91%
SBFR	0.81	84%	**0.83*** **	85%	**0.83**	86%	**0.83**	85%

Table 7
Producer's (PA) and user's (UA) accuracies for both species and PFTs at SERC across spatial resolutions (in %). Producer's accuracies represent the proportion of total pixels within a class that were correctly classified. User's accuracies represent the proportion classified as the correct class.

	Native		20 m		40 m		60 m	
Species	PA	UA	PA	UA	PA	UA	PA	UA
Crop	96	100	98	100	100	100	100	92
Crop residue/senesced grass	100	100	100	100	100	100	100	100
Acer spp.	49	46	62	80	100	100	–	–
Carya spp.	43	29	73	53	100	33	100	33
Fagus spp.	63	82	77	83	86	100	67	100
Liquidambar styraciflua	49	30	73	79	100	100	–	–
Liriodendron tulipifera	68	87	83	86	81	100	50	100
Platanus occidentalis	24	9	50	100	–	–	–	–
Quercus spp.	58	46	69	69	100	100	100	50
Pinus spp.	32	5	67	29	–	–	–	–
Soil	100	100	100	98	100	100	83	100
PFTs								
Annual herbaceous	96	100	99	100	100	100	100	92
Senesced annual herbaceous	100	100	100	100	100	100	100	100
Deciduous broadleaf tree	82	98	94	99	100	100	100	100
Evergreen needleleaf tree	45	3	67	15	–	–	–	–
Soil	100	100	100	100	100	100	83	100

Table 9
Producer's (PA) and user's (UA) accuracies for both species and PFTs at WR across spatial resolutions (in %).

	Native		20 m		40 m		60 m	
Species	PA	UA	PA	UA	PA	UA	PA	UA
Senesced grass	100	100	99	100	100	100	100	100
Acer circinatum	100	91	100	100	100	100	–	–
Acer macrophyllum	90	92	100	100	100	100	100	100
Alnus rubra	96	95	95	97	95	95	92	100
Populus trichocarpa	89	91	96	93	82	100	71	83
Abies grandis	36	1	0	–	0	–	–	–
Pseudotsuga menziesii	73	86	78	93	78	90	79	92
Thuja plicata	78	14	75	50	–	–	–	–
Tsuga heterophylla	81	74	92	76	94	79	93	75
Pteridium aquilinum	93	60	75	100	100	100	–	–
Rock and soil	100	85	100	100	–	–	–	–
PFTs								
Senesced annual herbaceous	100	100	100	100	98	100	100	100
Deciduous broadleaf shrub	100	86	100	100	100	100	–	–
Deciduous broadleaf tree	97	98	99	99	93	100	91	100
Evergreen needleleaf tree	100	100	100	100	100	98	100	98
Perennial herbaceous	93	59	75	100	100	100	–	–
Rock & soil	100	85	100	100	–	–	–	–

PFT user's accuracies also did not vary greatly across resolutions. These values were often slightly lower or very similar to the producer's accuracies for each PFT. One exception to this was the evergreen broadleaf tree class, for which user's accuracies were 11–16% higher than producer's accuracies.

3.3. Species classifications

Overall classification accuracies across sites and spatial resolutions ranged from 61.5% to 96.2% for dominant species (Table 12). As with PFT classifications, the overall accuracies achieved using native spatial resolution data were the lowest at all sites, except the GULF. The highest overall accuracies were at 40 m spatial resolution for four of the five study sites (SERC, WR, SBFR, and GULF). At SNEV, 60 m resolution data were the most accurately classified. The largest increases in overall accuracy between resolutions were between native and 20 m resolutions (1–14%), and significant ($p = 0.001$ or $p = 0.01$) increases in kappa were found for all sites. Differences in overall accuracy at coarser resolutions were small ($\pm$<3%) for all sites but SERC, where another significant ($p = 0.05$) increase in kappa was found between 20 and 40 m resolutions.

At SERC, species-level discrimination generally increased with coarsening spatial resolution, reaching a peak at 40 m resolution, and then stabilizing or decreasing at 60 m (Table 7). At 40 m resolution, seven of the nine remaining classes had producer's accuracies of 100% and eight of nine had user's accuracies of 100%. The largest increases (~13–57%) in producer's accuracies from native to 40 m resolution were found for tree species. Increases in user's accuracies, similar to those in producer's accuracies, were observed for several species; however, some species, such as hickory (*Carya* spp.) and oak (*Quercus* spp.) had much lower user's accuracies at 40 and 60 m resolutions.

Within the GULF species classification, producer's accuracies were ~90% or higher for all species except *J. roemerianus*, for which accuracy decreased sharply between 20 and 40 m resolutions (Table 8). Despite this decrease in producer's accuracy, user's accuracy for the species

Table 8
Producer's (PA) and user's (UA) accuracies for both species and PFTs at GULF across spatial resolutions (in %).

	Native		20 m		40 m		60 m	
Species	PA	UA	PA	UA	PA	UA	PA	UA
Avicennia germinans	–	–	96	100	91	99	89	96
Distichlis spicata	–	–	91	81	93	82	91	80
Juncus roemerianus	–	–	75	92	44	72	46	94
Phragmites australis	–	–	91	100	93	100	92	99
Spartina alterniflora	–	–	94	83	98	92	99	93
Spartina patens	–	–	98	90	97	97	97	96
Senesced vegetation	–	–	100	100	–	–	–	–
Clear water	–	–	100	100	–	–	–	–
Dark water	–	–	100	100	–	–	–	–
Sun glint	–	–	100	100	–	–	–	–
Muddy water	–	–	100	100	–	–	–	–
PFTs								
Evergreen broadleaf shrub	–	–	96	100	85	95	79	94
Perennial herbaceous	–	–	100	100	100	98	100	97
Senesced vegetation	–	–	100	100	–	–	–	–
Water	–	–	100	100	0	0	0	0

Table 10
Producer's (PA) and user's (UA) accuracies for both species and PFTs at SNEV across spatial resolutions (in %).

	Native		20 m		40 m		60 m	
Species	PA	UA	PA	UA	PA	UA	PA	UA
Quercus kelloggii	53	51	65	66	66	67	72	69
Salix spp.	85	84	83	100	100	100	100	100
Arctostaphylos spp.	59	54	78	64	85	64	77	68
Ceanothus cordulatus	78	65	96	87	89	100	100	100
Quercus chrysolepsis	59	30	74	45	57	42	40	40
Abies concolor	50	65	63	74	65	73	69	81
Abies magnifica	75	78	99	98	97	100	100	100
Calocedrus decurrens	50	21	57	56	72	81	50	60
Pinus jeffreyi	38	53	47	92	40	83	63	100
Pinus lambertiana	52	17	95	50	89	42	100	80
Pinus ponderosa	53	61	71	66	72	68	85	66
Sempervirens giganteum	42	5	43	50	100	100	0	0
Mixed meadow	98	100	99	100	100	100	98	100
Rock	93	99	96	100	91	100	94	100
PFTs								
Deciduous broadleaf tree	57	50	63	67	64	73	69	67
Evergreen broadleaf shrub	65	51	81	63	86	58	85	62
Evergreen broadleaf tree	63	28	78	43	64	45	60	50
Evergreen needleleaf tree	87	97	93	98	92	99	93	98
Annual herbaceous	98	99	99	100	100	100	98	100
Rock	93	99	96	100	91	100	94	100

Table 11
Producer's (PA) and user's (UA) accuracies for both species and PFTs at SBFR across spatial resolutions (in %).

	Native		20 m		40 m		60 m	
Species	PA	UA	PA	UA	PA	UA	PA	UA
Irrigated grasses	94	94	94	95	100	99	100	100
Brassica nigra	97	97	97	95	88	91	92	94
Mediterranean annual grasses and forbs	90	93	94	96	93	94	95	90
Platanus racemosa	87	85	82	84	95	95	97	100
Quercus douglasii	93	96	99	97	84	88	84	86
Artemisia californica-Salvia leucophylla	96	96	96	96	92	95	96	97
Arctostaphylos spp.	66	69	71	74	54	53	52	52
Baccharis pilularis	83	83	86	74	51	56	58	50
Ceanothus cuneatus	80	88	84	82	71	80	80	84
Ceanothus megacarpus	75	75	76	76	86	88	90	90
Ceanothus spinosus	71	74	69	71	86	87	89	85
Citrus spp.	97	96	96	97	98	99	98	95
Eucalyptus spp.	95	93	96	93	99	100	100	100
Persea americana	96	95	96	98	100	100	100	98
Quercus agrifolia	67	71	71	63	65	66	63	66
Umbellularia californica	79	82	82	79	84	89	93	92
Adenostoma fasciculatum	65	67	68	67	59	59	61	60
Eriogonum fasciculatum	97	98	98	99	93	96	95	95
Pinus sabiniana	42	48	44	51	73	79	76	76
Marsh/wetland	97	97	97	98	99	99	99	98
Rock	92	93	95	86	80	85	87	86
Bare soil	84	84	83	75	97	98	97	100
Urban	94	97	97	99	99	99	100	99
PFTs								
Annual herbaceous	98	98	98	98	96	96	96	94
Deciduous broadleaf tree	83	85	87	87	80	83	81	79
Drought-deciduous shrub	95	96	95	96	85	87	91	90
Evergreen broadleaf shrub	70	74	74	73	71	71	71	71
Evergreen broadleaf tree	80	82	82	79	92	93	93	96
Evergreen needleleaf shrub	76	76	78	79	71	72	72	73
Evergreen needleleaf tree	48	50	49	51	44	57	66	64
Perennial herbaceous	97	98	98	98	97	98	98	98
Rock & soil	91	92	92	88	90	92	94	94
Urban	93	96	96	99	99	100	100	99

remained high at both 20 and 60 m resolutions. User's accuracies for the other classes were also very high, being ≥70% at all spatial resolutions.

Species discrimination at the WR site was also quite high (producer's accuracies >70%) for all classes but the grand fir (*Abies grandis*) (Table 9). No strong pattern in producer's accuracies across spatial resolutions was evident for most species. For a few classes, one resolution was clearly the most accurate, such as black cottonwood (*Populus trichocarpa*) at 20 m resolution, or clearly least accurate, such as bracken fern (*Pteridium aquilinum*), also at 20 m resolution. An increase in producer's accuracies for the two most dominant species at this site, Douglas fir (*P. menziesii*) and western hemlock (*T. heterophylla*), both increased from native resolution to 20 m (by 5% and 11%, respectively). User's accuracies were similarly high and stable across resolutions for most species, with a few exceptions, such as *P. aquilinum*, for which accuracy increased greatly from native to 20 m resolution and *P. trichocarpa*, for which user's accuracy decreased almost 20% from 40 to 60 m resolution.

Table 12
Kappa coefficients and % overall accuracies (OA) for species classifications. Bold values indicate the highest kappa for each row. Asterisks denote significant differences from previous resolution (*p = 0.05, **p = 0.01, ***p = 0.001).

	Native		20 m		40 m		60 m	
Species	Kappa	OA	Kappa	OA	Kappa	OA	Kappa	OA
SERC	0.85	88%	0.89**	91%	**0.95***	96%	0.86	89%
GULF	–	–	0.90***	91%	**0.92**	94%	**0.92**	94%
WR	0.75	82%	0.83***	88%	**0.85**	88%	0.83	88%
SNEV	0.56	61%	0.71***	75%	0.72	76%	**0.76**	79%
SBFR	0.84	85%	**0.86*****	86%	**0.86**	86%	0.85	86%

At the SNEV site, we found higher variation in classification accuracies among species across spatial resolutions than at the other sites (Table 10). Classes with very high producer's and user's accuracies (>80% at all resolutions) included willow (*Salix* spp.) and meadow. Similar to the other sites, increases in producer's accuracies, ranging from 7% to 43%, were observed from native (here 3.3 m) to 20 m resolution for ten species. For several species (*Pinus ponderosa*, *Abies concolor* and *Q. kelloggii*), producer's accuracies continued to increase with coarsening spatial resolution. Producer's accuracies for other species decreased markedly from 40 to 60 m resolution. Unlike most species at other sites, many at SNEV reached a peak producer's accuracy at one spatial resolution. For example, at 20 m, *Q. chrysolepsis* achieved a producer's accuracy of 74%, 15–34% higher than at other resolutions. The optimum resolution also varied across species. User's accuracies were similar to producer's accuracies for some species and much lower for others. An initial increase in user's accuracies from native to 20 m resolution was observed for many of the same species, and the majority of species and cover classes had increasing user's accuracy with coarsened resolution. Overall, 60 m resolution data yielded the best producer's and user's accuracies, with 6 of 14 classes having accuracies ≥90%.

SBFR, the most diverse site with 23 species-level classes, was also well-classified (Table 11). Producer's accuracies greater than 90% at all spatial resolutions were achieved for eleven (ten plant species and URBAN) of these classes. Eight additional classes had producer's accuracies ranging from ~70% to 90% at all spatial resolutions. The results show high differentiation among species within and across PFTs. Only one class, *Pinus sabiniana*, a conifer which grows in sparse, often intermixed stands, had producer's accuracies 50% and lower. Overall, producer's accuracies for most species were very stable (±3%) across spatial resolutions, with just a few classes decreasing in accuracy at 60 m resolution. User's accuracies were also very stable across resolutions and tended to be either higher than producer's accuracies at all resolutions or lower at all resolutions across species.

4. Discussion

4.1. Species & PFT discrimination using coarse resolution data

In each of the five ecosystems included in this study, we were able to successfully discriminate both dominant plant species and PFTs at coarser resolutions (≥20 m). The average overall accuracy for classifications at these resolutions was 87% at the species-level and 94% at the PFT-level. We also observed changes in classification accuracy across spatial resolutions, with patterns that varied by site. Given the differences in site composition and class, species and PFT diversity, our results demonstrate that coarser resolution imaging spectroscopy data can be used to reliably classify most dominant species and PFTs within each ecosystem. Though, there are many ecosystem types that were not included in this study, and these may prove more challenging to map (e.g., a desert ecosystem with very low vegetation cover). Still, these results generally corresponded well with imaging spectroscopy studies in similar ecosystems (e.g., Dennison & Roberts, 2003; Plourde et al., 2007; Roberts et al., 2004; Swatantran, Dubayah, Roberts, Hofton, & Blair, 2011). The most frequent source of classification error for species at any site was confusion among species within the same PFT or among species that spatially co-occur. Confusion among PFTs at each site was very low. These results support using imaging spectrometer data for dominant species and PFT classification, as compared to other global broadband sensors of similar spatial resolution, such as Landsat. For example, Goodenough et al. (2003) found classifying dominant species and PFTs using imaging spectrometer data from Hyperion to be 15% more accurate than with Landsat-7 ETM+ data. In urban areas, Herold & Roberts (2006) compared simulated coarse resolution broadband IKONOS and AVIRIS data for classifying land cover, finding AVIRIS to be less sensitive than IKONOS to coarsening spatial resolution due to its greater spectral coverage and finer spectral resolution.

4.2. Impact of varying spatial resolution

The most prominent change we observed in overall accuracy across changing spatial resolutions was an increase from native (3.3–12 m) to 20 m resolutions. This was observed at all sites and for both species and PFT classifications, with the exception of the GULF site, for which we had no data finer than 20 m. In fact, at sites with finer native resolutions (i.e., SERC, SNEV and WR), we observed the greatest increases in accuracy up to 20 m, though this did not hold true for the PFT classification at WR, in which accuracy remained high and very stable over all resolutions. These increases are consistent with previous multi-scale classification studies using multispectral imagery (e.g., Chen et al., 2004; Marceau, Gratton, et al., 1994; Treitz & Howarth, 2000). The effect of changing spatial resolution on class-specific producer's and user's accuracies varied across sites. The provided maps of SBFR and SNEV sites illustrate the endpoints of this continuum. At SBFR, we observed little to no change in both distribution and accuracy for both species (Fig. 3) and PFTs (Fig. 4) across spatial resolutions. In the SNEV species maps (Fig. 5), we see how inter-mixed (i.e., potentially confused) dominant species are at native (3.3 m) spatial resolution. With coarser resolutions, dominant patches become more clearly defined, but most of the fine-scale species variation is lost. While less change occurs for PFTs than for species (Fig. 6), we do see that some classes, such as annual herbaceous meadows that are relatively small and interspersed, are lost at coarser resolutions. In general, there are three major factors driving these changes in accuracy across spatial resolutions: patch characteristics, within-class spectral variability and reference data limitations.

Class patch characteristics played an important role in classification success. We hypothesized that the highest accuracies would be achieved when the image spatial resolution most closely approximated a class' patch size and would decrease as edge pixels are averaged in at coarser resolutions. Patch size ultimately determines at what resolution a species or PFT can be resolved as dominant. Classes with small patch sizes relative to pixel size were not classifiable at coarser resolutions (e.g., *L. styraciflua* at SERC or *P. aquilinum* and *Acer circinatum* at WR). Obeysekera and Rutchey (1997) found similar results when mapping Everglades' vegetation at a range of scales. Losing classes at coarser resolution is expected, but represents an important limitation of hard-classified, coarse resolution maps, beyond classification accuracy. Though a class may not be dominant at a particular scale (i.e., no pixels composed of 70% or more of this class), it may still be dominant within the site (e.g., present in all pixels). This introduced bias toward more spatially dominant classes is further discussed in Boschetti, Flasse, and Brivio (2004) and Latifovic and Olthof (2004) and is a critical consideration for map users. Not only is patch size a factor, but also shape (i.e., better to minimize edges). Large isodiametric or block-shaped patches of a species will be more spatially resistant to changing resolutions than species whose patches tend to be long and thin (i.e., lots of edge to area; Fig. 7) (Chen et al., 2004). For example, at SBFR, marsh reference patches were large and semi-rectangular (>120 m by 120 m), and its classification accuracy changed very little across resolutions (0.5–1%). Contrast this with *Plantanus racemosa* in the riparian zones at this site, where accuracy decreased sharply with coarsening spatial resolution. This relationship between patch characteristics and spatial scale in classification is well-documented within the object-based analysis literature (Blaschke, 2010). Some examples include studies by Hall, Hay, Bouchard, and Marceau (2004) and Hay, Marceau, and Dub (2001), who generated patch objects at a range of scales to determine how patch types changed as a result of resolution. Furthermore, Hay, Niemann, and Goodenough (1997) demonstrated that the spatial pattern of patches in a landscape directly influence the optimal spatial resolution for mapping them accurately. Image native resolution also plays a key role in determining the effects of scaling on the accuracy of mapping. A recent study by Karl and Maurer (2009), using IKONOS & Landsat data to compare multi-scale estimates of vegetation cover from image segmentation and pixel aggregation, found the native resolution of the imagery was a factor in identifying patch boundaries (i.e., Landsat data were not able to represent the edges of irregularly-shaped or small patches as clearly as the finer resolution IKONOS data could). This inability to capture these patches at native resolution translated to greater error at coarser resolutions.

Accurate discrimination among classes relies on our ability to minimize within-class spectral variance while at the same time maximizing between-class variance. Spatial resolution is one of the primary controls on within-class spectral variance, as it defines which components of the scene are represented at the pixel-scale (Woodcock & Strahler, 1987). At the finest resolutions, a canopy is a collection of leaves, branches, potentially exposed substrate and shadows. At slightly coarser scales, we resolve sunlit and shadowed crown as well as canopy gaps, making crown geometry an important factor in spectral variance (Asner, 1998; Cohen et al., 1990). The detection of separate canopy components contributes to higher within-class variance, potentially resulting in lower pixel-based accuracies (Clark et al., 2005). Spatial averaging, as in this study, results in the mean spectrum for each class remaining relatively stable (up to a certain resolution), while the variance decreases at each successive resolution (Blan & Butler, 1999; Chen et al., 2004; Marceau, Howarth, & Gratton, 1994). Fig. 8 illustrates this decrease for *A. concolor* from the SNEV site.

This decrease in variance may explain the observed increase in classification accuracies from native to 20 m resolution found in this study. Increases in accuracy beyond 20 m may indicate that within-class variance is still high at 20 m resolution. As mentioned previously, we can expect the highest accuracies to occur when the spatial resolution most closely approximates patch size, meaning within-class variance is at a minimum while local spatial variance is at a maximum (Marceau, Howarth, et al., 1994). When patch sizes vary across the

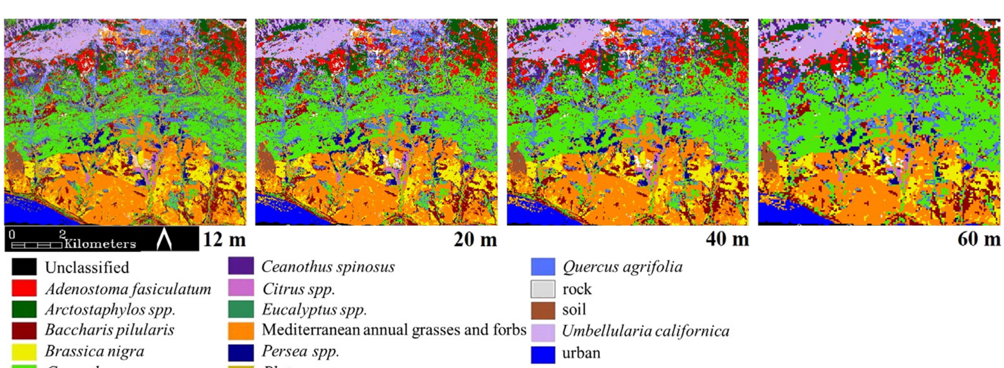

Fig. 3. Subset of the dominant species classification maps for all spatial resolutions at the SBFR site.

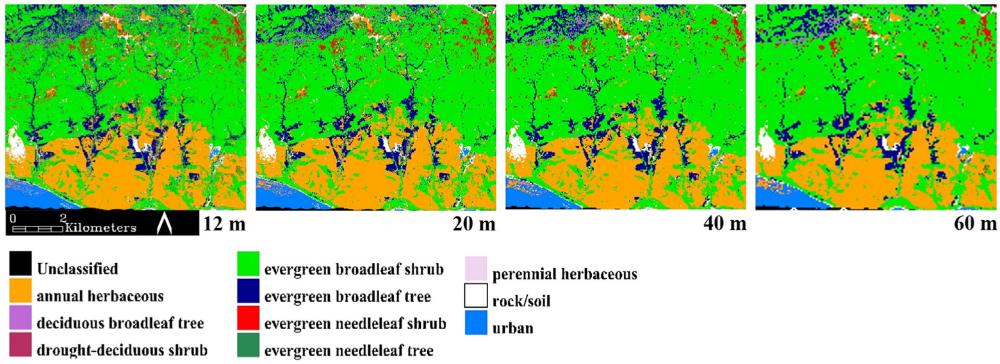

Fig. 4. Subset of the PFT classification maps for all spatial resolutions at the SBFR site.

image, it can be challenging to find an optimal pixel scale. Object-oriented approaches overcome this issue by using a pixel majority filter at the crown scale, thus producing higher accuracies by ignoring some pixel-scale errors. Examples include work by Clark et al. (2005) in tropical forests, and Myint, Gober, Brazel, Grossman-Clarke, and Weng (2011) and Alonzo et al. (2013) in urban areas. For forested ecosystems, such as WR and SNEV, reduced within-canopy variance is likely a major contributing factor to improvements in accuracy at coarser resolutions. At SNEV, many of the dominant species have somewhat open canopies, growing in stands with many gaps composed of soil, litter and understory species (Swatantran et al., 2011). At 3.3 m resolution, canopy shadows and gaps are major contributors to the spectral diversity of these classes. At WR, we observed another example of reduced within-class variance at coarser resolutions leading to improved accuracies. At native resolution (4 m), some bright sunlit canopy pixels that belonged primarily to Douglas fir (*P. menziesii*) were classified as *P. aquilinum*, an herbaceous perennial species. At 20 m, these brighter pixels were averaged out, decreasing *P. menziesii* spectral variance, and thus leading to better discrimination between these classes. Given these observations, differentiating species using pixel-based classification will likely be more successful with coarser resolution data (≥20 m).

The reference data collected and used for this study also played a role in modulating changes in accuracy across resolutions. Dominance was assigned at the patch (i.e., polygon), not pixel, scale, and each patch contained from one to thousands of pixels from the native images. In order for a patch to be considered dominated by a particular class, that polygon needed to be composed of 70% or more that class. However, all pixels within a reference patch were assigned to the dominant class. This means that as many as 30% of the pixels in each polygon might have been dominated by another class. For species that frequently grow intermixed, these co-dominant pixels may have been accurately classified, but were calculated as errors due to the identification of the polygon they fell within. At coarser resolutions, averaging increased the dominant's spectral signal strength, leading to more pixels being “accurately” classified. In these cases, the increase we observed in accuracy from native to 20 m may not actually exist, because the native resolution accuracy is underreported. At SBFR, for example, chamise (*Adenostoma fasciculatum*) and manzanita (*Arctostaphylos* spp.) commonly grow in mixtures ranging from 40/60 to 60/40. Confusion among these two species in our classifications was common, but accuracies for both classes increased with coarsening spatial resolution. The same issue arises for forest gaps, which may not be well-defined in the reference data. For example, at WR, gaps are dominated by *P. aquilinum* or *A. circinatum*, and these gaps may be resolved at 4 m resolution. However, gap pixels correctly classified as *P. aquilinum* or *A. circinatum* in these areas will be counted as classification errors given the reference polygon label (Fig. 9).

The composition of reference patches also contributes to the training spectral signature of a class. While the small random training sample size used in this study should ensure a higher likelihood that the “real” dominant's spectra make up the majority of the signature, for some cases in which the same species are always intermixed, this increases the chances that the class training signatures will also be a blend. One example of this is the high level of confusion between *Quercus agrifolia* and *Umbellularia californica* at SBFR, where mixed patches of these two species dominate the north-facing slopes (and south facing riparian areas at high elevation) and as such, *Q. agrifolia* classification accuracy tends to be relatively lower (Table 11). Another example of potentially mixed training signatures are the evergreen needleleaf tree species at SNEV, particularly incense cedar (*C. decurrens*), ponderosa pine (*P. ponderosa*) and sugar pine (*Pinus lambertiana*) which often are so intermixed that they are

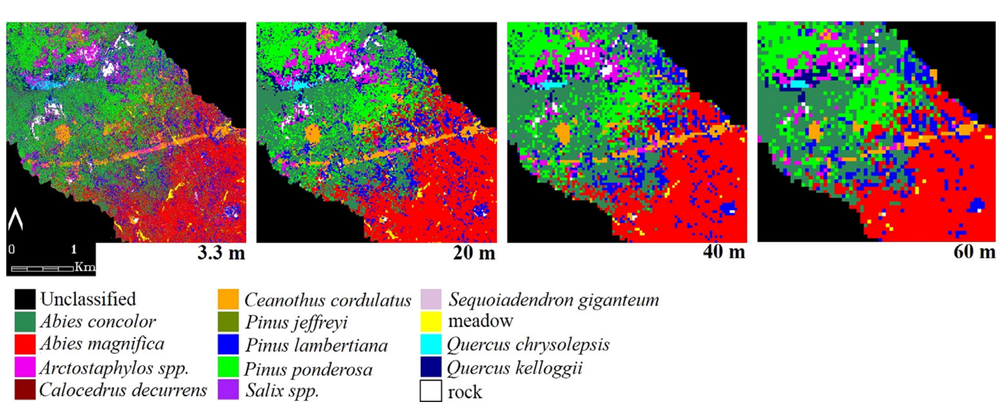

Fig. 5. Subset of the dominant species classification maps for all spatial resolutions at the SNEV site.

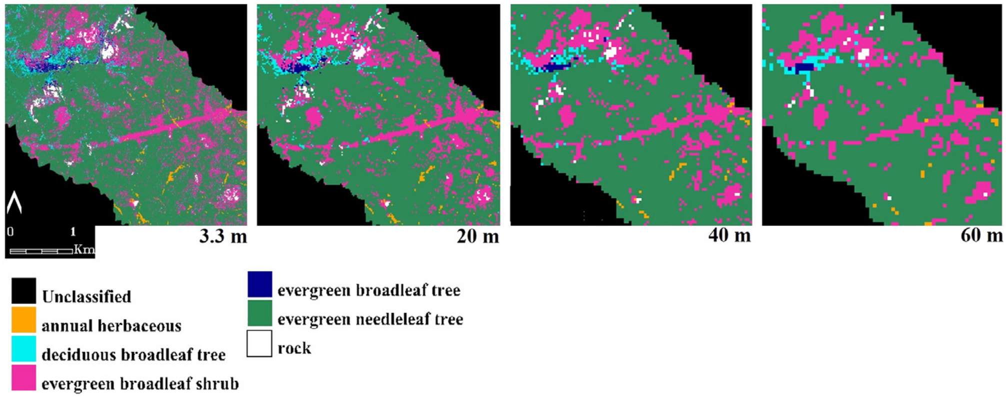

Fig. 6. Subset of the PFT classification maps for all spatial resolutions at the SNEV site.

most frequently mapped as "Sierran mixed conifer" in other studies (e.g., Swatantran et al., 2011). Finally, the delineation of reference patches also influences the impact of edge pixels as resolution is coarsened. If patches are delineated to be as large as possible (e.g., WR, SERC), then edge pixels are likely to be dominated by another class. However, if reference patches are delineated within an even larger patch of the same class (e.g., SBFR), then the averaging of edge pixels will have a lower impact on the classification results. The inclusion or exclusion of edge pixels from the reference polygons at coarser resolutions most certainly impacts the reported accuracies. As previously stated, edge pixels do not necessarily mean mixed pixels, but the frequency of mixed pixels will be higher in more fragmented landscapes (Powell et al., 2004). In this study, some edge pixels were incorporated, but not all, as is evidenced by the loss of reference polygons and even entire classes at some resolutions (Fig. 2). The exclusion of some edge pixels means that we have not fully represented this error in our accuracy assessment and have somewhat biased it toward more dominant classes. Powell et al. (2004) found a significant decrease in accuracy when all edge pixels were included in the assessment. However, they also state that it is difficult to assign this error to either incorrect reference data or a classification error. This issue is a common one in the classification of remote sensing data because land cover classes rarely have hard boundaries, and sometimes the mixture of two classes may resemble a third, entirely different class.

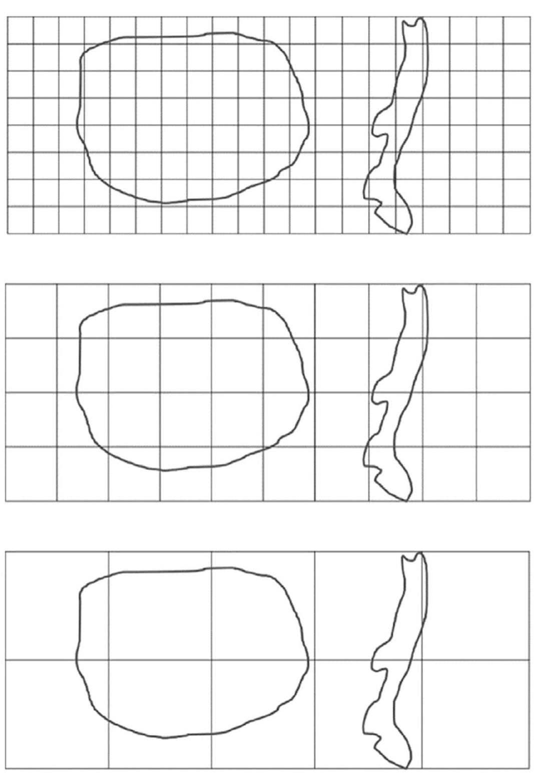

Fig. 7. Illustration demonstrating how patch shape impacts the included pixels across resolutions. In the top frame, the right polygon would include 46 pixels, and the left would include 7. In the middle frame, the right polygon would include 12 pixels, and the left would include 3. In the bottom frame, the right polygon would include 4 pixels and the left would include 0.

4.3. Using fine scale training data

As mentioned previously, collecting high quality reference data for dominant species and PFTs across a landscape is a challenge for many mapping efforts (Foody & Mathur, 2006). The results of this study support the use of fine scale reference spectra to classify dominant plant species and PFTs on coarser resolution imagery. This is critical given that the majority of reference data available will come from regional fine resolution (~3–18 m) imaging spectrometer data sets. These data can provide a wealth of reference spectra for use with coarser global hyperspectral coverage, providing spectral information for the many species and PFTs whose spatial distribution makes extracting this data at 30 or 60 m unlikely. It is important to note that we did not test training libraries extracted at coarse resolutions in this study. However, Schaaf et al. (2011) found that training spectra extracted from fine resolution (~3–18 m) AVIRIS performed better for classifying coarse resolution images than did training data extracted at coarse resolution. Building reference training data from finer resolution sources has also proven successful in other studies, especially when classes of interest do not occur as pure pixels within the imagery (e.g., DeFries et al., 1998; Roberts et al., 2012). One potential challenge to using fine resolution data may be matching the seasonality, something that was not considered in this study. Further studies, such as that by Dudley, Dennison, Roth, Roberts, & Coates (2015), are needed to assess the portability of

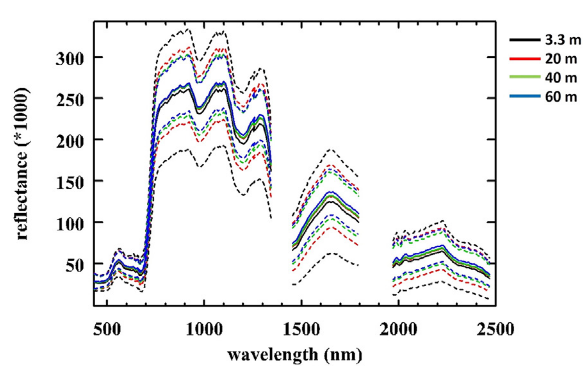

Fig. 8. Mean (solid) and ±1 standard deviation (dashed) spectra for *Abies concolor* across all four spatial resolutions.

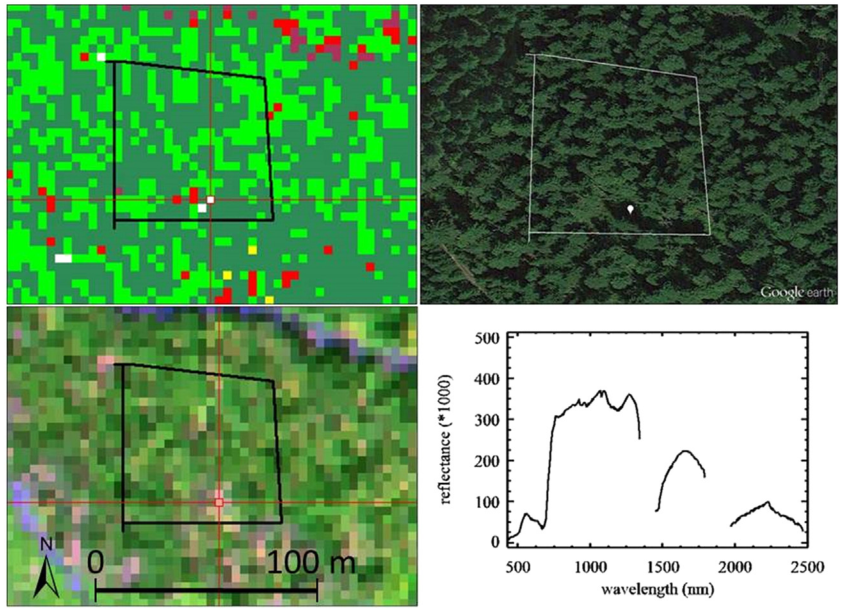

Fig. 9. Forest gap in *Pseudotsuga menziesii* stand classified as *Acer circinatum* at WR. Upper left panel shows the classification image, where white pixels are *Acer circinatum* and light green are *Pseudotsuga menziesii*. The red crosshairs highlight one pixel that has been classified as *Acer circinatum* within the *Pseudotsuga menziesii* polygon (outlined in black). Lower left panel is a false color composite of the AVIRIS image (R = 1652 nm, G = 826 nm, B = 665 nm) with red crosshairs on the same pixel. Upper right panel is a close up of the stand in Google Earth with a white marker on the same area as the pixel of interest. Lower right panel is the AVIRIS spectrum from this pixel. (For interpretation of the references to color in this figure legend, the reader is referred to the web version of this article.)

spectra in time. Another point to consider is spectral mixing among classes. While some classes disappear at coarser resolutions, they are still occurring with the same frequency within an image. They have become part of a mixture of species or PFTs (the analog to associations in floristic mapping). These mixtures may still be spectrally unique, but will no longer have the same training signature developed from fine resolution library. Depending on the classifier used, results over these mixtures will likely differ greatly. In this study, no pixels were classified as these "disappeared" classes. Indeed, these species are no longer dominant at this scale, so the results are accurate from that perspective. However, it is important to consider what is meant by dominant and how this relates to a given objective or application when creating these maps.

5. Conclusions

In this study, we sought to evaluate the impact of spatial resolution on our ability to accurately map plant species and PFTs using imaging spectrometer data. By spatially aggregating fine resolution airborne AVIRIS data (~3–18 m) to subsequently coarser spatial resolutions (20–60 m), we simulated data such as those to be acquired globally by sensors currently in development. We performed our analysis over five ecosystems containing a wide diversity of both plant species and PFTs. Furthermore, we evaluated the potential for using training data derived from fine resolution imagery to classify species and PFTs at coarser resolutions. Our results show that the best classification accuracies were found at coarser resolutions, rather than native. These results coincide with similar studies of scale in remote sensing which found the optimal mapping resolution occurs when within class spectral variance is lowest and classes have not yet begun to mix spatially (i.e., the resolution closely approximates class patch size). Because of this, the ideal spatial resolution will vary based on both the diversity and distribution of species and PFTs in an ecosystem. However, our findings show that, at all sites considered, 20 through 60 m spatial resolution is acceptable for mapping ecosystem-level dominant species and PFTs. This means the 30 m and 60 m resolutions proposed for upcoming sensors like EnMAP and HyspIRI should sufficient for mapping dominant species and PFTs. The impact of changes in spatial resolution varied mainly among classes within ecosystems rather than across ecosystems. Class patch size and spatial distributions were critical factors in determining accuracy at a given resolution. In ecosystems with small, fragmented patches of dominant species or PFTs, maps at coarser resolution no longer contained some of the original classes. Thus it is important for users to understand what is meant by 'dominant' in any given classification map and the implications this may have on particular map uses. The use of a small sample of fine resolution training data to classify species and PFTs at all resolutions was successful, meaning that spectral libraries created from regional studies will likely be applicable to coarser resolution space-borne hyperspectral data.

Several directions for future research are clear. Firstly, more realistic simulation and up-scaling of fine spatial resolution data will help improve assessments of the potential applications of coarse resolution spaceborne imaging spectrometers. The spatial averaging used in this study does not accurately simulate the sampling point-spread-function of proposed sensors or preserve the signal to noise ratio across resolutions. Studies manipulating the up-scaling of images have also found this aggregation technique impacts the spatial structure of the resulting images (e.g., Chen & Henebry, 2009). The observations made in this study should be compared to results using other pixel- and object-based classifiers to gain a broader understanding of the likely impact of resolution on species and PFT mapping on a global scale. Furthermore, many studies have shown that moving toward the incorporation of sub-pixel composition (e.g., species diversity, PFT fraction, etc.) is also a promising direction (e.g., Rocchini, McGlinn, Ricotta, Neteler, & Wohlgemuth, 2011; Schmidtlein et al., 2012). Incorporating land surface phenology (i.e., seasonality) could also improve discrimination among species and PFTs (Dennison & Roberts, 2003; Dudley et al., 2015), especially those that have contrasting phenologies. Seasonal data will exist with spaceborne sensors, and thus its influence on accuracy should be assessed.

Accurate maps of PFT and species composition are invaluable for a range of scientific applications. While the scale of use for each of the applications may vary, currently proposed spaceborne imaging spectrometers promise the best opportunity to create these maps worldwide. At regional scales, they can be used for biodiversity monitoring, land management decision-making and ecosystem process modeling, but may not be well-suited for applications such as detecting invasive species. At continental to global scales, these maps will provide more consistent and reliable reference data for building global land cover products, tracking land cover change and climate modeling. The proposed spatial resolutions for these sensors are fine enough to map dominant plant species and PFTs across diverse ecosystems. Finally, promising new initiatives for collecting the necessary reference data for creating these maps (e.g., NASA's Ecological Spectral Information System) are coming online, and should be ready and operational upon the launch of a spaceborne imaging spectrometer.

Acknowledgments

We would like to thank everyone who helped collect the reference data used in this research, especially Geoffrey Parker, Gregory Fryer, Michael Toomey and Bree Belyea. Special thanks to NASA JPL AVIRIS team for collecting and providing the image data. Funding for this study was provided by NASA grants NNX12AP08G, HyspIRI discrimination of plant species and functional types along a strong environmental-temperature gradient and NNX08AM89G, Spatial, Spectral and Temporal Requirements for Improved Hyperspectral Mapping of Plant Functional Types, Plant Species, Canopy Biophysics and Canopy Biochemistry, and in part by a proposal to the NSF Rapid Grant Program entitled "Analysis of NASA's Advanced Visible Infrared Imaging Spectrometer Data Acquired Over Multiple Dates and Flight lines along the Northern Gulf Coastline, including Barrier Islands," (Principal Investigator S. Ustin). We would also like to thank the two anonymous reviewers who took the time to provide excellent feedback in revising this article.

References

Alonzo, M., Roth, K., & Roberts, D. A. (2013). Identifying Santa Barbara's urban tree species from AVIRIS imagery using canonical discriminant analysis. *Remote Sensing Letters*, *4*(5), 513–521.

Asner, G. P. (1998). Biophysical and biochemical sources of variability in canopy reflectance. *Remote Sensing of Environment*, *64*(3), 234–253.

Asner, G. P. (2013). Biological diversity mapping comes of age. *Remote Sensing*, *5*(1), 374–376.

Atkinson, P. M., & Curran, P. J. (1995). Defining an optimal size of support for remote sensing investigations. *IEEE Transactions on Geoscience and Remote Sensing*, *33*(3), 768–776.

Atkinson, P. M., & Curran, P. J. (1997). Choosing an appropriate spatial resolution for remote sensing investigations. *Photogrammetric Engineering and Remote Sensing*, *63*(12), 1345–1351.

Blan, L., & Butler, R. (1999). Comparing effects of aggregation methods on statistical and spatial properties of simulated spatial data. *Photogrammetric Engineering and Remote Sensing*, *65*(1), 73–84.

Blaschke, T. (2010). Object based image analysis for remote sensing. *ISPRS Journal of Photogrammetry and Remote Sensing*, *65*(1), 2–16.

Bonan, G. B., Levis, S., Kergoat, L., & Oleson, K. W. (2002). Landscapes as patches of plant functional types: an integrating concept for climate and ecosystem models. *Global Biogeochemical Cycles*, *16*(2).

Boschetti, L., Flasse, S. P., & Brivio, P. A. (2004). Analysis of the conflict between omission and commission in low spatial resolution dichotomic thematic products: the PARETO boundary. *Remote Sensing of Environment*, *91*(3–4), 280–292.

Chen, D., Stow, D. A., & Gong, P. (2004). Examining the effect of spatial resolution and texture window size on classification accuracy: an urban environment case. *International Journal of Remote Sensing*, *25*(11), 2177–2192.

Chen, W., & Henebry, G. M. (2009). Change of spatial information under rescaling: a case study using multi-resolution image series. *ISPRS Journal of Photogrammetry and Remote Sensing*, *64*(6), 592–597.

Clark, M. L., Roberts, D. A., & Clark, D. B. (2005). Hyperspectral discrimination of tropical rain forest tree species at leaf to crown scales. *Remote Sensing of Environment*, *96*(3–4), 375–398.

Cochrane, M. A. (2000). Using vegetation reflectance variability for species level classification of hyperspectral data. *International Journal of Remote Sensing*, *21*(10), 2075–2087.

Cohen, W. B., Spies, T. A., & Bradshaw, G. A. (1990). Semivariograms of digital imagery for analysis of conifer canopy structure. *Remote Sensing of Environment*, *34*(3), 167–178.

Congalton, R. G. (1991). A review of assessing the accuracy of classifications of remotely sensed data. *Remote Sensing of Environment*, *37*(1), 35–46.

Curran, P. J., & Atkinson, P. M. (1999). Issues of scale and optimal pixel size. *Spatial Statistics for Remote Sensing*, *1*. (pp. 115–133). Kluwer Academic.

DeFries, R. S., Hansen, M., Townshend, J. R. G., & Sohlberg, R. (1998). Global land cover classifications at 8 km spatial resolution: the use of training data derived from Landsat imagery in decision tree classifiers. *International Journal of Remote Sensing*, *19*(16), 3141–3168.

DeFries, R. S. (2008). Terrestrial vegetation in the coupled human-earth system: contributions of remote sensing. *Annual Review of Environment and Resources*, *33*(1), 369–390.

DeFries, R. S., Field, C. B., Fung, I., Justice, C. O., Los, S., Matson, P. A., ... Vitousek, P. M. (1995). Mapping the land-surface for global atmosphere-biosphere models — toward continuous distributions of vegetation functional-properties. *Journal of Geophysical Research - Atmospheres*, *100*(D10), 20867–20882.

Dennison, P. E., & Roberts, D. A. (2003). The effects of vegetation phenology on endmember selection and species mapping in southern California chaparral. *Remote Sensing of Environment*, *87*(2–3), 295–309.

Dudley, K. L., Dennison, P. E., Roth, K. L., Roberts, D. A., & Coates, A. R. (2015). A multi-temporal spectral library approach for mapping vegetation species across spatial and temporal phonological gradients. *Remote Sensing of Environment*, *167*, 121–134.

Feld, C. K., da Silva, P. M., Sousa, J. P., De Bello, F., Bugter, R., Grandin, U., ... Harrison, P. (2009). Indicators of biodiversity and ecosystem services: a synthesis across ecosystems and spatial scales. *Oikos*, *118*(12), 1862–1871.

Féret, J. B., & Asner, G. P. (2012). Tree species discrimination in tropical forests using airborne imaging spectroscopy. *IEEE Transactions on Geoscience and Remote Sensing*, *51*(1), 1–12.

Fisher, P. (1997). The pixel: a snare and a delusion. *International Journal of Remote Sensing*, *18*(3), 679–685.

Fisher, R. A. (1936). The use of multiple measurements in taxonomic problems. *Annals of Eugenics*, *7*(2), 179–188.

Foody, G. M., & Mathur, A. (2006). The use of small training sets containing mixed pixels for accurate hard image classification: training on mixed spectral responses for classification by a SVM. *Remote Sensing of Environment*, *103*(2), 179–189.

Friedl, M. A., McIver, D. K., Hodges, J. C. F., Zhang, X. Y., Muchoney, D., Strahler, A. H., ... Schaaf, C. (2002). Global land cover mapping from MODIS: algorithms and early results. *Remote Sensing of Environment*, *83*(1–2), 287–302.

Goodenough, D. G., Dyk, A., Niemann, K. O., Pearlman, J. S., Chen, H., Han, T., ... West, C. (2003). Processing Hyperion and ALI for forest classification. *IEEE Transactions on Geoscience and Remote Sensing*, *41*(6), 1321–1331.

Göttlicher, D., Obregón, A., Homeier, J., Rollenbeck, R., Nauss, T., & Bendix, J. (2009). Land-cover classification in the Andes of southern Ecuador using Landsat ETM+ data as a basis for SVAT modelling. *International Journal of Remote Sensing*, *30*(8), 1867–1886.

Green, R. O., Eastwood, M. L., Sarture, C. M., Chrien, T. G., Aronsson, M., Chippendale, B. J., ... Olah, M. R. (1998). Imaging spectroscopy and the Airborne Visible Infrared Imaging Spectrometer (AVIRIS). *Remote Sensing of Environment*, *65*(3), 227–248.

Hall, O., Hay, G. J., Bouchard, A., & Marceau, D. J. (2004). Detecting dominant landscape objects through multiple scales: an integration of object-specific methods and watershed segmentation. *Landscape Ecology*, *19*(1), 59–76.

Hansen, M. C., DeFries, R. S., Townshend, J. R. G., & Sohlberg, R. (2000). Global land cover classification at 1 km spatial resolution using a classification tree approach. *International Journal of Remote Sensing*, *21*(6), 1331–1364.

Harvey, K. R., & Hill, G. J. E. (2001). Vegetation mapping of a tropical freshwater swamp in the Northern Territory, Australia : a comparison of aerial photography, Landsat TM and SPOT satellite imagery. *International Journal of Remote Sensing*, *22*(15), 2911–2925.

Hay, G. J., Marceau, D. J., & Dub, P. (2001). A multiscale framework for landscape analysis : object-specific analysis and upscaling. *Landscape Ecology*, *16*(2001), 471–490.

Hay, G. J., Niemann, K. O., & Goodenough, D. G. (1997). Spatial thresholds, image-objects, and upscaling : a multiscale evaluation. *Remote Sensing of Environment*, *62*, 1–19.

Herold, M., & Roberts, D. A. (2006). Multispectral Satellites - Imaging Spectrometry — LIDAR: Spatial - Spectral Tradeoffs in Urban Mapping. *International Journal of Geoinformatics*, *2*(1), 1–13.

HyspIRI Science Team (2009). *NASA 2008 HyspIRI White Paper and Workshop Report.* , 79 (Pasadena, CA).

Kalacska, M. R., Bohlman, S. A., Sanchez-Azofeifa, G. A., Castro-Esau, K., & Caelli, T. (2007). Hyperspectral discrimination of tropical dry forest lianas and trees: comparative data reduction approaches at the leaf and canopy levels. *Remote Sensing of Environment*, *109*(4), 406–415.

Karl, J. W., & Maurer, B. A. (2009). Multivariate correlations between imagery and field measurements across scales: comparing pixel aggregation and image segmentation. *Landscape Ecology*, *25*(4), 591–605.

Kaufmann, H., Segl, K., Chabrillat, S., Hofer, S., Stuffler, T., Mueller, A., ... Back, H. (2006). EnMAP — a hyperspectral sensor for environmental mapping and analysis. *Proceedings of the IEEE International Geoscience and Remote Sensing Symposium, Denver, Colorado* (pp. 1617–1619).

Kerr, J. T., & Ostrovsky, M. (2003). From space to species: ecological applications for remote sensing. *Trends in Ecology & Evolution*, *18*(6), 299–305.

Klecka, W. (1980). *Discriminant analysis.* SAGE University Press (71 pp.).

Kokaly, R. F., Asner, G. P., Ollinger, S. V., Martin, M. E., & Wessman, C. A. (2009). Characterizing canopy biochemistry from imaging spectroscopy and its application to ecosystem studies. *Remote Sensing of Environment*, *113*(Supplement 1), S78–S91.

Kokaly, R. F., Despain, D. G., Clark, R. N., & Livo, K. E. (2003). Mapping vegetation in Yellowstone National Park using spectral feature analysis of AVIRIS data. *Remote Sensing of Environment*, *84*(3), 437–456.

Latifovic, R., & Olthof, I. (2004). Accuracy assessment using sub-pixel fractional error matrices of global land cover products derived from satellite data. *Remote Sensing of Environment*, *90*(2), 153–165.

Li, L., Ustin, S. L., & Lay, M. (2005). Application of multiple endmember spectral mixture analysis (MESMA) to AVIRIS imagery for coastal salt marsh mapping: a case study in China camp, CA, USA. *International Journal of Remote Sensing*, *26*(23), 5193–5207.

Loveland, T. R., Reed, B. C., Brown, J. F., Ohlen, D. O., Zhu, Z., Yang, L., & Merchant, J. W. (2000). Development of a global land cover characteristics database and IGBP DISCover from 1 km AVHRR data. *International Journal of Remote Sensing*, *21*(6–7), 1303–1330.

Marceau, D. J., Gratton, D. J., Fournier, R. A., & Fortin, J. P. (1994a). Remote-sensing and the measurement of geographical entities in a forested environment 2. The optimal spatial-resolution. *Remote Sensing of Environment*, *49*(2), 105–117.

Marceau, D. J., Howarth, P. J., & Gratton, D. J. (1994b). Remote sensing and the measurement of geographical entities in a forested environment 1. The scale and spatial aggregation problem. *Remote Sensing of Environment*, *49*(2), 93–104.

Martin, M. E., Newman, S. D., Aber, J. D., & Congalton, R. G. (1998). Determining forest species composition using high spectral resolution remote sensing data. *Remote Sensing of Environment*, *65*(3), 249–254.

Muchoney, D., Strahler, A., Hodges, J., & LoCastro, J. (1999). The IGBP DISCover confidence sites and the system for terrestrial ecosystem parameterization: tools for validating global land-cover data. *Photogrammetric Engineering and Remote Sensing*, *65*(9), 1061–1067.

Myint, S. W., Gober, P., Brazel, A., Grossman-Clarke, S., & Weng, Q. (2011). Per-pixel vs. object-based classification of urban land cover extraction using high spatial resolution imagery. *Remote Sensing of Environment*, *115*(5), 1145–1161.

National Research Council (2007). *Earth Science and Applications from Space: National Imperatives for the Next Decade and Beyond.* (456 pp.).

Nelson, M. D., McRoberts, R. E., Holden, G. R., & Bauer, M. E. (2009). Effects of satellite image spatial aggregation and resolution on estimates of forest land area. *International Journal of Remote Sensing*, *30*(8), 1913–1940.

Obeysekera, J., & Rutchey, K. (1997). Selection of scale for Everglades landscape models. *Landscape Ecology*, *12*(1), 7–18.

Pengra, B. W., Johnston, C. A., & Loveland, T. R. (2007). Mapping an invasive plant, *Phragmites australis*, in coastal wetlands using the EO-1 Hyperion hyperspectral sensor. *Remote Sensing of Environment*, *108*(1), 74–81.

Plourde, L. C., Ollinger, S. V., Smith, M. L., & Martin, M. E. (2007). Estimating species abundance in a northern temperate forest using spectral mixture analysis. *Photogrammetric Engineering and Remote Sensing*, *73*(7), 829–840.

Powell, R., Matzke, N., de Souza, C., Clark, M., Numata, I., Hess, L., & Roberts, D. (2004). Sources of error in accuracy assessment of thematic land-cover maps in the Brazilian Amazon. *Remote Sensing of Environment*, *90*(2), 221–234.

Price, K. P., Guo, X., & Stiles, J. M. (2002). Optimal Landsat TM band combinations and vegetation indices for discrimination of six grassland types in eastern Kansas. *International Journal of Remote Sensing*, *23*(23), 5031–5042.

Pu, R. L. (2009). Broadleaf species recognition with in situ hyperspectral data. *International Journal of Remote Sensing*, *30*(11), 2759–2779.

Richter, R., & Schläpfer, D. (2002). Geo-atmospheric processing of airborne imaging spectrometry data. Part 2: Atmospheric/topographic correction. *International Journal of Remote Sensing*, *23*(13), 2631–2649.

Roberts, D. A., Green, R. O., & Adams, J. B. (1997). Temporal and spatial patterns in vegetation and atmospheric properties from AVIRIS. *Remote Sensing of Environment*, *62*(3), 223–240.

Roberts, D. A., Ustin, S. L., Ogunjemiyo, S., Greenberg, J., Dobrowski, S. Z., Chen, J., & Hinckley, T. M. (2004). Spectral and Structural Measures of Northwest Forest Vegetation at Leaf to Landscape Scales. *Ecosystems*, *7*(5), 545–562.

Roberts, D. A., Quattrochi, D. A., Hulley, G. C., Hook, S. J., & Green, R. O. (2012). Synergies between VSWIR and TIR data for the urban environment: an evaluation of the potential for the Hyperspectral Infrared Imager (HyspIRI) decadal survey mission. *Remote Sensing of Environment*, *117*, 83–101.

Rocchini, D., McGlinn, D., Ricotta, C., Neteler, M., & Wohlgemuth, T. (2011). Landscape complexity and spatial scale influence the relationship between remotely sensed spectral diversity and survey-based plant species richness. *Journal of Vegetation Science*, *22*(4), 688–698.

Roth, K. L., Dennison, P. E., & Roberts, D. A. (2012). Comparing endmember selection techniques for accurate mapping of plant species and land cover using imaging spectrometer data. *Remote Sensing of Environment*, *127*, 139–152.

Roth, K. L., Roberts, D. A., Dennison, P. E., Alonzo, M., Peterson, S. H., & Beland, M. (2015). Evaluating strategies for discriminating plant species within and across diverse ecosystems with imaging spectroscopy. *Remote Sensing of Environment*, *167*, 135–151.

Schaaf, A. N., Dennison, P. E., Fryer, G. K., Roth, K. L., & Roberts, D. A. (2011). Mapping plant functional types at multiple spatial resolutions using imaging spectrometer data. *GIScience and Remote Sensing*, *48*(3), 324–344.

Schaepman, M. E., Ustin, S. L., Plaza, A. J., Painter, T. H., Verrelst, J., & Liang, S. (2009). Earth system science related imaging spectroscopy—an assessment. *Remote Sensing of Environment*, *113*(Supplement 1), S123–S137.

Schmidtlein, S., Feilhauer, H., & Bruelheide, H. (2012). Mapping plant strategy types using remote sensing. *Journal of Vegetation Science*, *23*(3), 395–405.

Somers, B., & Asner, G. P. (2013). Invasive species mapping in Hawaiian rainforests using multi-temporal Hyperion spaceborne imaging spectroscopy. *IEEE Journal of Selected Topics in Applied Earth Observations and Remote Sensing*, *6*(2), 351–359.

Sun, W. X., & Liang, S. (2008). Methodologies for mapping plant functional types. In S. Liang (Ed.), *Advances in Land Remote Sensing* (pp. 369–393). Springer.

Sun, W. X., Liang, S. L., Xu, G., Fang, H. L., & Dickinson, R. (2008). Mapping plant functional types from MODIS data using multisource evidential reasoning. *Remote Sensing of Environment*, *112*(3), 1010–1024.

Swatantran, A., Dubayah, R., Roberts, D. A., Hofton, M., & Blair, J. B. (2011). Mapping biomass and stress in the Sierra Nevada using lidar and hyperspectral data fusion. *Remote Sensing of Environment*, *115*(11), 2917–2930.

Treitz, P., & Howarth, P. (2000). High spatial resolution remote sensing data for forest ecosystem classification an examination of spatial scale. *Remote Sensing of Environment*, *72*(3), 268–289.

Turner, D. P., Ollinger, S. V., & Kimball, J. S. (2004). Integrating remote sensing and ecosystem process models for landscape- to regional-scale analysis of the carbon cycle. *Bioscience*, *54*(6), 573–584.

Turner, M. G., Neill, R. V. O., Gardner, R. H., & Milne, T. B. (1989). Effects of changing spatial scale on the analysis of landscape pattern. *Landscape Ecology*, *3*(3/4), 153–162.

Turner, W., Spector, S., Gardiner, N., Fladeland, M., Sterling, E., & Steininger, M. (2003). Remote sensing for biodiversity science and conservation. *Trends in Ecology & Evolution*, *18*(6), 306–314.

Underwood, E. C., Ustin, S. L., & Ramirez, C. M. (2007). A comparison of spatial and spectral image resolution for mapping invasive plants in coastal California. *Environmental Management*, *39*(1), 63–83.

Ustin, S. L., & Gamon, J. A. (2010). Remote sensing of plant functional types. *New Phytologist*, *186*(4), 795–816.

Ustin, S. L., Adams, J. B., Elvidge, C. D., Rejmanek, M., Rock, B. N., Smith, M. O., ... Woodward, R. A. (1986). Thematic mapper studies of semiarid shrub communities. *Bioscience*, *36*(7), 446–452.

Ustin, S. L., Roberts, D. A., Gamon, J. A., Asner, G. P., & Green, R. O. (2004). Using imaging spectroscopy to study ecosystem processes and properties. *Bioscience*, *54*(6), 523.

Van Aardt, J., & Wynne, R. H. (2007). Examining pine spectral separability using hyperspectral data from an airborne sensor: an extension of field-based results. *International Journal of Remote Sensing*, *28*(1–2), 431–436.

Woodcock, C. E., & Strahler, A. H. (1987). The factor of scale in remote sensing. *Remote Sensing of Environment*, *21*(3), 311–332.

Wu, H., & Li, Z. L. (2009). Scale issues in remote sensing: a review on analysis, processing and modeling. *Sensors*, *9*(3), 1768–1793.

Zhang, C., & Qiu, F. (2012). Mapping individual tree species in an urban forest using airborne lidar data and hyperspectral imagery. *Photogrammetric Engineering and Remote Sensing*, *78*(10), 1079–1087.